Hyper-Rayleigh scattering from the bulk of nominally pure $KTaO_3$

H. Vogt
Max-Planck-Institut für Festkörperforschung, Heisenbergstrasse 1, Postfach 80 06 65, D-7000 Stuttgart 80, Federal Republic of Germany
(Received 5 July 1989)

Second-harmonic light or hyper-Rayleigh scattering from the bulk of nominally pure $KTaO_3$ is studied as a function of scattering configuration and temperature between 10 and 200 K. At the lower end of the temperature range the selection rules on the polarizations of incident and scattered light are similar to those of the soft-mode hyper-Raman line, while at the upper end they become reminiscent of hyper-Raman scattering by longitudinal-optical phonons. For any scattering configuration the temperature dependence of the intensity is given by $(A+B\Omega_0^{-2})^2$, where the soft-mode frequency Ω_0 is the only parameter varying with temperature. We interpret our results in terms of symmetry-breaking microregions formed by quasistatic lattice distortions around a defect core. Hyper-Rayleigh scattering turns out to be unspecific with respect to the core, but to probe the activation of hyper-Raman tensors by the quasistatic lattice distortions and the associated macroscopic electric field. We compare our results with recent observations of noncubic local symmetry in $KTaO_3$.

I. INTRODUCTION

Since the beginning of hyper-Raman spectroscopy,[1-3] it has been pointed out that the elastic or quasielastic line at twice the laser frequency can be even weaker than the hyper-Raman lines, disturbing the observation of low-frequency optical phonons less seriously than the Rayleigh line in ordinary Raman scattering. This advantage is particularly expected for centrosymmetric crystals. Here, the second-order susceptibility $\chi^{(2)}$ vanishes within the dipole approximation and hence does not permit coherent second-harmonic generation (SHG) followed by ordinary Rayleigh scattering. Moreover, $\chi^{(2)}$ cannot be induced by the elastic strains of acoustic phonons or by entropy fluctuations and similar quasistatic excitations of even parity, so that the corresponding scattering processes, e.g., hyper-Brillouin scattering, are forbidden by symmetry.

Nevertheless, a hyper-Rayleigh line seems to be unavoidable and, to the best of our knowledge, has been detected in all cases where hyper-Raman scattering has unambiguously been identified. Unfortunately, a large variety of mechanisms contributing to hyper-Rayleigh scattering can be imagined so that it is rather difficult to single out the correct one. Introductory remarks on the mechanisms will be postponed to Sec. II for the sake of clarity.

There are at least two reasons why attention should be focused on hyper-Rayleigh scattering from cubic oxygen perovskites.

(a) As a by-product of soft-mode investigations, it has been found that the hyper-Rayleigh lines of these materials show a temperature dependence somehow resembling that of the static dielectric constants.[4-6] A detailed analysis of this effect, however, has not yet been given, although Levanyuk *et al.*[7] have proposed a phenomenological description extending their theory of light scattering from imperfect crystals into the nonlinear regime.[8-10]

(b) There are numerous indications of noncubic local symmetry even in nominally pure crystals. For example, Sokoloff *et al.*[11] have observed a central peak in the ordinary Raman and Brillouin spectra of cubic $BaTiO_3$ which they interpreted as evidence for dynamic polar clusters of precursor tetragonal order. Maglione *et al.*[12] have measured a Debye-type dielectric dispersion of $SiTiO_3$ and $KTaO_3$ in the radio-frequency range which they associated with the crossover from a displacive to an order-disorder behavior predicted by the well-known model of interlinked double-minimum potentials. From their NMR data, Rod *et al.*[13] concluded that the Ta ions in $KTaO_3$ sit in a noncubic environment on a time scale of 10^{-7} sec or longer below about 40 K. Uwe *et al.*[14] introduced the concept of symmetry-breaking microregions in order to explain the first-order features in the Raman spectrum of $KTaO_3$. We expect that hyper-Rayleigh scattering can be related to the results just quoted because it also probes deviations from the cubic symmetry, at least on a time scale determined by the maximum resolution of our spectrometer, i.e., about 10^{-10} sec. Let us stress, however, that the overall cubic symmetry is not questioned at all, but is assumed to hold if an average is taken over a sufficiently large time interval or crystal volume.

In this paper we concentrate on nominally pure $KTaO_3$. We measure the hyper-Rayleigh intensity as a function of the scattering geometry and determine its temperature dependence between 10 and 200 K. Although the hyper-Rayleigh line might result entirely from lattice imperfections, it turns out to be mainly characterized by properties of the $KTaO_3$ host lattice. This is not surprising for a highly polarizable medium in which lattice imperfections are surrounded by lattice distortions extending over many unit cells. Indeed, formulas derived by various authors[7-10,15] for elastic scattering from

"frozen impurities" near structural phase transitions essentially express the response of the host lattice and contain only two quite unspecific defect parameters, i.e., the defect concentration and the strength of the coupling between defect core and host lattice at their interface.

We have divided our subject matter into four sections. In order to facilitate the discussion of our results, we summarize preliminary ideas about hyper-Rayleigh scattering mechanisms in Sec. II. In Sec. III we present our experimental data. There, we include the temperature dependence of the soft-mode hyper-Raman intensity which we use as reference, especially when comparing hyper-Rayleigh intensities from different samples. Finally, in Sec. IV we interpret our findings in terms of quasistatic optical-phonon–type lattice distortions and the hyper-Raman tensors activated by them.

Throughout the paper, elastic line, central component, hyper-Rayleigh, and second-harmonic light scattering are used as synonyms. HRL and HRM are chosen as abbreviations of hyper-Rayleigh and hyper-Raman, respectively.

II. HYPER-RAYLEIGH SCATTERING MECHANISMS IN CRYSTALS

A. SHG related mechanisms

In general, it is not very useful to study HRL scattering from crystals lacking a center of inversion because the dominant effect will be SHG followed by ordinary Rayleigh scattering of the second-harmonic light. For similar reasons we should avoid backward or forward scattering geometries where SHG at the surface of the sample can interfere with the proper HRL line.

In centrosymmetric crystals we have to take into account SHG due to nonlinear source terms involving the spatial gradient of the exciting electric field. These source terms may be lumped together to an effective nonlinear polarization of the form[16]

$$\mathbf{P}_{\text{eff}}^{\text{NL}}=\chi^{\text{NL}}:\mathbf{k}_L\mathbf{E}_L\mathbf{E}_L \ , \tag{1}$$

where $\mathbf{k}_L$ and $\mathbf{E}_L$ represent the wave vector and the electric field of the incident laser radiation, respectively, and χ^{NL} is an appropriate fourth-rank tensor. In isotropic media $\mathbf{P}_{\text{eff}}^{\text{NL}}$ is always parallel to $\mathbf{k}_L$ and no second-harmonic light can be generated propagating parallel to the fundamental wave.[16] In anisotropic media this happens if $\mathbf{k}_L$ is restricted to highly symmetric directions, e.g., $\langle 100\rangle$ and $\langle 110\rangle$ in cubic crystals. Then a purely longitudinal nonlinear polarization wave is left. In 90° scattering configurations it might contribute to the HRL line and, indeed, has been referred to for explaining HRL scattering from rutile.[3,17]

B. Intrinsic versus defect-induced mechanisms

Besides the nonlinear polarization waves induced in any crystal, there are two main categories of HRL mechanisms, i.e., intrinsic odd-parity excitations of very low-frequency and disturbances of the inversion symmetry by lattice imperfections. Examples of the former are encountered in molecular crystals as relaxator-type modes associated with an order-disorder phase transition or the melting process. They could clearly be identified as dynamical origin of central components whenever their spectral linewidth considerably exceeded the instrumental resolution of typically a few cm^{-1}.[18–20] On the other hand, the HRL lines observed for crystals of simple structure, e.g., alkali halides[3,21] and CaF_2 (Ref. 22), seem to arise unquestionably from defects and static distortions of the surrounding host lattices, although some hopping mobility of the defects on time scales inaccessible to HRM spectroscopy cannot be excluded *a priori*.

For a number of materials undergoing structural phase transitions, several authors did not dare to decide which of the two categories just stated applies.[23–25] The spectral width cannot be resolved by a conventional double monochromator, whereas the temperature dependence of the intensity reveals some relation to the order parameter or its mean square deviation.

C. Mechanisms in $KTaO_3$

In the case of $KTaO_3$ we can readily imagine two kinds of low-frequency odd-parity excitations which might be involved in the central component: (i) Soft-mode contributions to acoustic phonons resulting from quasiharmonic or anharmonic mode coupling, and (ii) hopping motions of the central Ta ions within a multiwell potential.

The coupling of acoustic phonons and the soft mode in $KTaO_3$ has been well established.[26–28] At the center of the Brillouin zone, however, it is based on the *quadratic* relation between the acoustic strain and the soft-mode polarization provided by the electrostrictive coefficients.[26] The acoustic phonons cannot activate the HRM tensor of the soft mode by this effect, which mainly presents a damping mechanism for both phonon types. In order to obtain a linear mixing of phonon amplitudes we have to refer to the quasiharmonic coupling describing the phonon eigenvectors at finite wave vectors of $\mathbf{q}$ in terms of the phonon eigenvectors at $\mathbf{q}=0$.[27] Now the coupling parameters become quadratic in the components of $\mathbf{q}$. In our light scattering experiments $\mathbf{q}$ may be too small for observing a contribution to the soft mode ($\mathbf{q}=0$) to the acoustic phonons ($\mathbf{q}\neq 0$) and a corresponding hyper-Brillouin scattering, the intensity of which should depend on the fourth power of the wave vector. In fact, the quasiharmonic mode coupling does not account for any of our present experimental results.

Hopping motions between off-center positions of the Ta ions have not yet been proven to be definitely intrinsic excitations of pure $KTaO_3$ since the indications of noncubic symmetry quoted in Sec. I have been interpreted with partly conflicting models. Quasistatic lattice distortions probed by HRL scattering can arise from either lattice imperfections or intrinsic off-center displacements. As long as the cubic overall symmetry is not violated, the two cases cannot be distinguished by our technique. Nevertheless, we should look for thermal hysteresis effects and variations of the absolute HRL intensity from sample to sample. Both kinds of observations may indi-

cate that lattice imperfections are operative.[6,25]

Since the time scale of the quasistatic lattice distortions, either defect-induced or intrinsic, is expected to be large compared to the periods of the acoustic phonons with wave vectors given by the scattering configuration,[13] hyper-Brillouin scattering can no longer be strictly excluded by the parity arguments of the Introduction and may appear like the first-order Raman features.[14] As an effect of higher order, however, it will contribute to the unresolved central component much less than the proper HRL scattering.

III. EXPERIMENTAL DETAILS AND RESULTS

A. Experimental setup

The essential part of our experimental arrangement is sketched in Fig. 1. As a source of the exciting radiation we use an acousto-optically Q-switched Nd-YAG laser (pulse repetition rate 5 kHz, energy per pulse 0.5 mJ). The laser power can be attenuated without change of mode structure by a combination of a half-wave plate ($\lambda/2$) and two Glan prisms (GP). The polarization of the laser light is rotated by a motor-driven half-wave plate ($m-\lambda/2$), the angular position of which is monitored by the power traversing the GP behind the sample (S). An $f/1$ objective with a focal length of 7.5 cm collects the scattered light while a Dove prism (DP) rotates the image of the laser beam so that it becomes parallel to the entrance slit of the spectrometer. We use the first stage of a double monochromator as a spectrograph and a position-sensing photomultiplier tube (ITT-F4146 M, Mepsicron) as an optical multichannel detector. The analog output of the position computer specifying the spectral elements of the impinging photons is fed to a pulse height analyzer (PHA). We gate the multichannel detection system by operating the PHA in the sampling mode. Since the position computer yields pulses of 8-

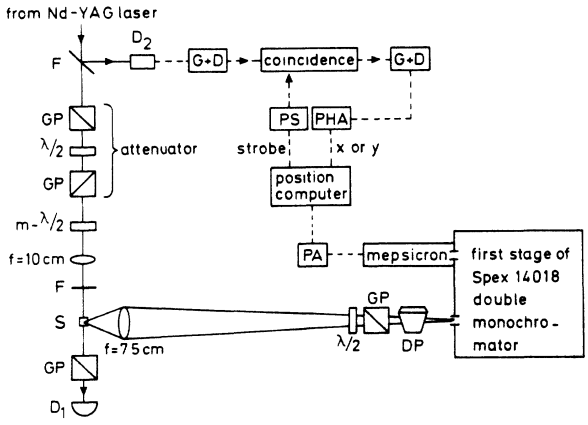

FIG. 1. Experimental setup. F, Schott filter RG850; GP, Glan prism; $\lambda/2$, half-wave plate; m-$\lambda/2$, motor-driven half-wave plate; S, sample; D_1, power meter; D_2, photodiode; DP, Dove prism; PA, preamplifier; PS, pulse shaper; G+D, gate and delay generator; PHA, pulse height analyzer.

μsec duration, additional care has to be taken to prevent photon pulses generated within 8 μsec before a laser pulse from contributing to the dark current. This is achieved by a coincidence circuit ensuring that the PHA only accepts photon pulses released from the photocathode during the 150-nsec width of a laser shot.

Measurements are performed on four single crystals of $KTaO_3$ grown from a K_2O-rich solution by two different techniques at two different laboratories.[29] Samples are sawed and ground to cubes with {100} and {110} surfaces and 3–5-mm edge lengths. They are mounted in a continuous-flow cryostat and cooled by helium exchange gas. The temperature is deduced from the anti-Stokes to Stokes intensity ratio of the soft-mode HRM scattering intensity. This method is particularly favored by the strong decrease of the soft-mode frequency with temperature and ceases to be applicable below 8 K and above 200 K.

Typical results of our measurements are presented in Fig. 2. The left side shows the temperature dependence of the triplet consisting of the anti-Stokes and Stokes HRM lines of the soft mode and the central component. On the right side the integral HRL intensity is plotted as a function of the laser polarization defined by the angle ϕ between the electric field of the laser and the [010] or y axis of the sample. We find a drastic change of both the intensity and the selection rules of HRL scattering with temperature.

In order to exclude that the observed HRL scattering

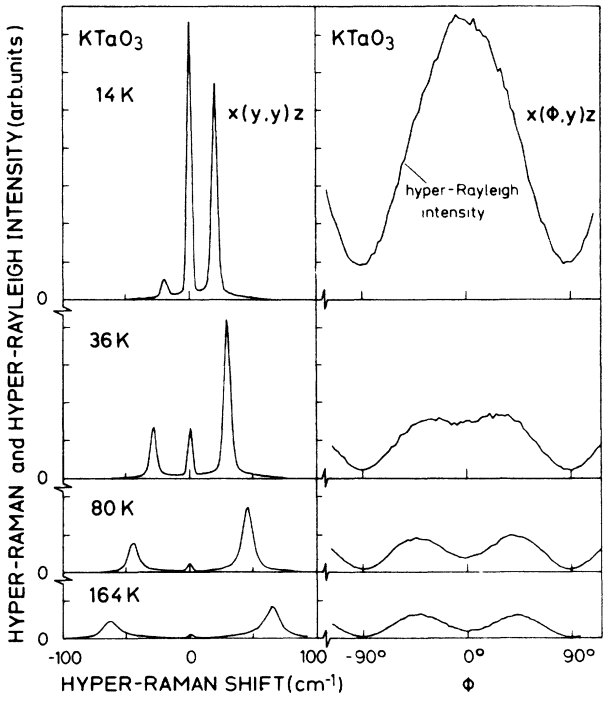

FIG. 2. Essential features of hyper-Rayleigh scattering from $KTaO_3$. Left side, temperature dependence of the triplet resulting from hyper-Rayleigh and soft-mode hyper-Raman scattering; right side, integral hyper-Rayleigh intensity as a function of the laser polarization defined by the angle between the electric field of the laser light and the [010] direction of the sample.

is influenced by SHG at surfaces or arises from gross imperfections, e.g., inclusions of air or particles, we exploit the two-dimensional capabilities of our multichannel detector and measure the distribution of the HRL and soft-mode HRM intensity along the entrance slit of the spectrometer or the path of the laser beam through the sample, respectively. The result is shown in Fig. 3, demonstrating an almost constant HRL to HRM intensity ratio within the indicated region selected for our analysis. The maxima on the right are due to an imperfect polishing of the rear surface conspicuous to the naked eye.

B. Soft-mode results

Since the multichannel detection reduces the time required for taking a HRM spectrum between -100 and $+100\ \mathrm{cm}^{-1}$ to less than 10^3 sec, we are now able to determine the HRM intensity as a function of temperature in detail, keeping the laser intensity constant during a whole cycle of measurements. Our experimental data are plotted in the lower part of Fig. 4. In the upper part we add the temperature dependence of the soft-mode frequency $\Omega_0(T)$ which we shall often refer to. Our present $\Omega_0(T)$ is in agreement with previous reports[5] and can be well described by Barrett's formula[5] as indicated by the solid line.

According to the general expression for HRM efficiencies,[30] the soft-mode HRM intensity I_{HRM} depends on four parameters which may vary with temperature. Besides Ω_0, we have to take into account the Bose-Einstein population factor n, the refractive index η, and the HRM tensor element a operative in the scattering configuration $x(yy)z$, where x, y, and z denote the cubic axes of $KTaO_3$. Regarding the temperature dependence of η as negligible[31] or incorporating it into that of an effective value of a, we may write

$$I_{\mathrm{HRM}}(T)\sim\begin{cases}\dfrac{a^2(n+1)}{\Omega_0} & \text{for the Stokes line ,}\\[2ex] \dfrac{a^2 n}{\Omega_0} & \text{for the anti-Stokes line .}\end{cases}\tag{2}$$

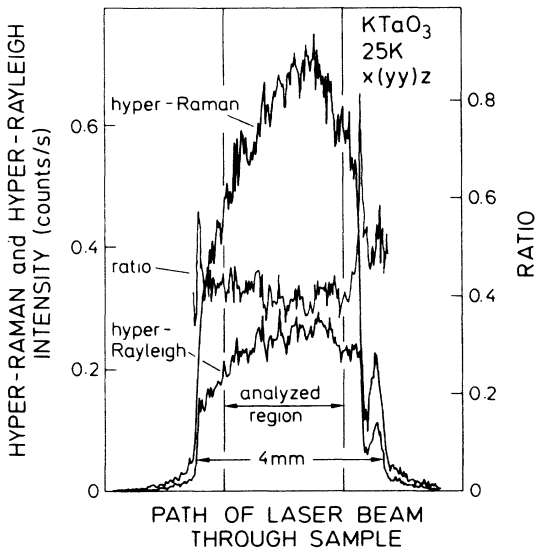

FIG. 3. Distribution of hyper-Rayleigh and soft-mode hyper-Raman intensity (Stokes component) along the entrance slit of the spectrometer or the path of the laser beam inside the sample.

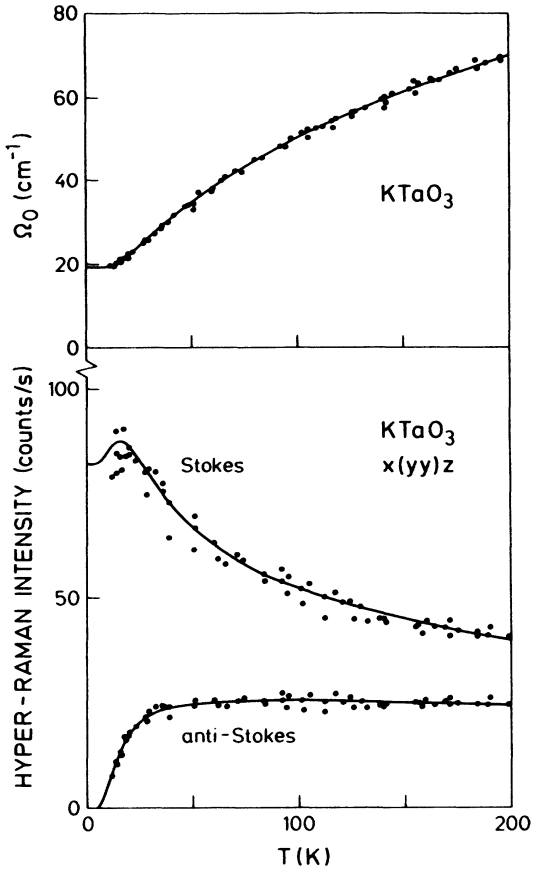

FIG. 4. Frequency Ω_0 and hyper-Raman intensities of the soft mode as function of temperature. Solid line in the upper part, Barrett's formula; solid line in the lower part, Eq. (2) if Barrett's formula and the straight line in Fig. 5 are taken for $\Omega_0(T)$ and $a(T)$, respectively.

Figure 5 shows $|a(T)|$ as derived from the experimental results of Fig. 4 by means of Eq. (2). There is a slight decrease of $|a|$ with increasing temperature. Approximating $|a(T)|$ and $\Omega_0(T)$ by a straight line and Barrett's formula, respectively, we obtain $I_{\mathrm{HRM}}(T)$ from Eq. (2) as depicted by the solid curves in the lower part of Fig. 4. We have also determined the ratio a/b of the two soft-mode HRM tensor elements[30,32] as function of temperature by comparing the HRM intensities measured for the scattering configurations $x(yy)z$ and $x(zy)z$. We observe a slight decrease of a/b from 2.9 at 10 K to 2.4 at 300 K.

Since the temperature dependence of the HRM tensor elements is not very pronounced. Figures 4 and 5 do not seriously affect the general statement that $I_{\mathrm{HRM}}(T)$ is given by $n(T)$ and $\Omega_0(T)$, becoming proportional to Ω_0^{-2}

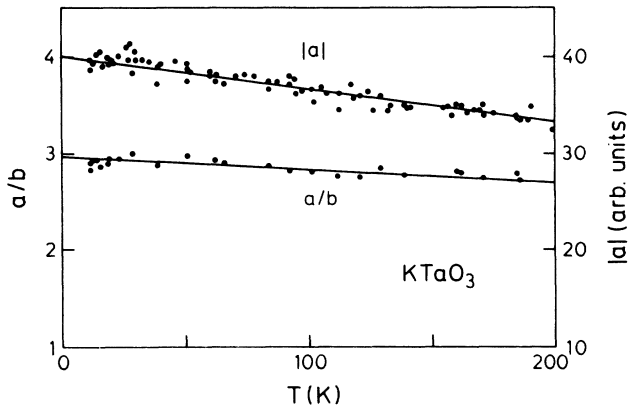

FIG. 5. Temperature dependence of the hyper-Raman tensor elements of the soft mode.

in the high-temperature limit.[6,32,33]

Finally, Fig. 6 shows the low-frequency part of the HRM spectrum at 6 and 14 K obtained for the scattering configurations $x(yy)\bar{x}$ and $x(yy)z$, respectively. As our multichannel detector system does not permit us to narrow the spectral slit width below about 3 cm^{-1}, we must return to the conventional single-channel technique[24] for achieving the indicated spectral resolution. Probably due to surface effects, the HRL line for the unfavorable backscattering geometry $x(yy)\bar{x}$ is almost three times more intense than that for $x(yy)z$.

We have included Fig. 6 in order to emphasize three points.

(i) The shape of the HRL line coincides with the instrumental profile thus yielding no information about the natural width.

(ii) We do not find any indication for a dynamical coupling between the central component and the soft-mode HRM line. The time scales of the corresponding processes are well separated.

(iii) According to the Lyddane-Sachs-Teller relation the infrared contribution to the static dielectric constant at low temperatures must be around 4400. It exceeds the value derived in Ref. 12 from the radio-frequency dielectric dispersion by an order of magnitude.

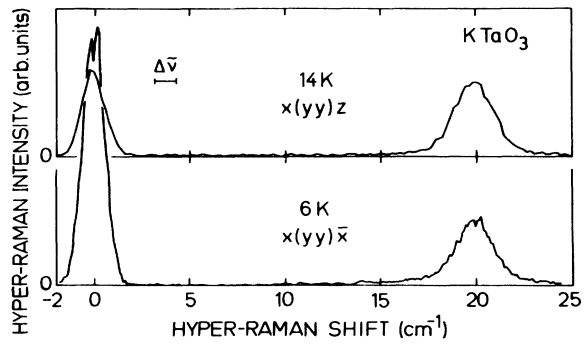

FIG. 6. Hyper-Rayleigh and soft-mode hyper-Raman lines at low temperatures. Note the different scattering geometries.

C. Results on hyper-Rayleigh scattering

In Fig. 7 we plot the square root of the HRL intensity as a function of temperature. The integral soft-mode HRM intensity is always used as reference, the measured ratio of HRL and HRM intensities being multiplied by the standard HRM intensity, the Stokes and anti-Stokes contributions to which are presented in Fig. 4. The solid curves are fits of the expression $A+B\Omega_0^{-2}$ to the experimental points where the parameters A and B do not depend on temperature, but only on the scattering configuration. Thus the temperature dependence of the HRL intensity I_{HRL} can be described by

$$I_{\mathrm{HRL}}(T)=[A+B/\Omega_0^2(T)]^2 . \tag{3}$$

At low temperatures I_{HRL} varies like Ω_0^{-4} or the square of the phonon contribution to the static dielectric constant. This behavior has been predicted in Ref. 7 and is also found for the intensity of electric-field-induced SHG.[32,35] Since the Stokes intensity of soft-mode HRM scattering varies with a smaller power of $1/\Omega_0$, it will be overtaken by I_{HRL} when Ω_0 has decreased sufficiently.

Additionally, Fig. 7 shows that the ratio of the HRL intensities observed for $x(yy)x$ and $x(zy)z$ approaches the corresponding ratio of the soft-mode HRM intensities given by $(a/b)^2$. Hence we should be able to express the selection rules of HRL scattering at low temperatures in terms of the HRM tensor of the soft mode.

The third piece of information we can extract from Fig. 7 concerns the influence of lattice imperfections. Comparing the $x(yy)z$ curves for samples 1 and 2, we find the ratio of HRL and HRM intensities to vary from sample to sample by a noticeable factor, although the temper-

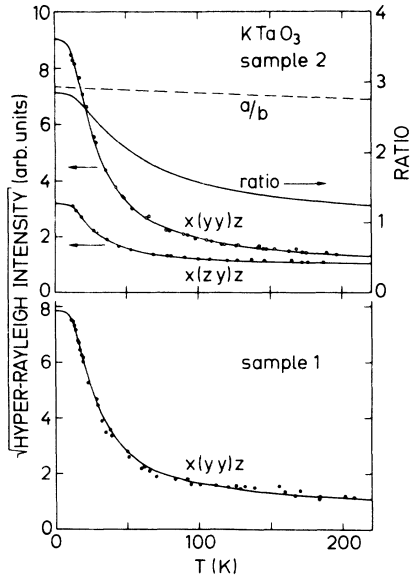

FIG. 7. Square root of the integral hyper-Rayleigh intensity observed for two scattering geometries and two samples as a function of temperature. Solid circles, cooling; open circles, heating. The solid lines represent fits of Eq. (3) to the experimental points.

ature dependence remains the same. The factor is between 1 and 1.7 if we compare four samples in equivalent scattering configurations. This observation seems to indicate that lattice imperfections of varying concentrations have to be considered as the origin of HRL scattering. On the other hand, thermal hysteresis effects as encountered in the paraelectric phases of $BaTiO_3$ and $KNbO_3$ (Refs. 4, 6, and 33) are absent between 10 and 300 K [see the solid and open circles in the $x(yy)z$ curve for sample 2 referring to cooling and heating, respectively].

Finally, Fig. 8 shows the HRL intensity as a function of the laser polarization at the lower and upper end of the temperature interval under study. The [101] and [$\bar{1}$01] directions are denoted by x' and z', respectively. Again, the low-temperature results are reminiscent of the soft mode,[30] the differences between HRL and HRM scattering being slight, but characteristic, as will be explained in the following section. The high-temperature curves are similar to those obtained for HRM scattering by longitudinal-optic (LO) phonons.[30]

IV. INTERPRETATION

A. Expressions for the hyper-Rayleigh scattering efficiency

The strength of HRL scattering is characterized by the ratio of the scattering efficiency S_{HRL} (differential scattering cross section per unit volume) and the exciting laser intensity I_L. In analogy to the expression for HRM scattering,[30] we find

$$\frac{S_{\mathrm{HRL}}}{I_L}=\frac{2\pi}{c\eta}\left[\frac{2\omega_L}{c}\right]^4 V|\hat{\mathbf{e}}_S\cdot\chi^{(2)}(\mathbf{q}):\hat{\mathbf{e}}_L\hat{\mathbf{e}}_L|^2 . \quad (4)$$

Here, ω_L is the laser frequency, V the scattering volume, and $\mathbf{q}$ the wave vector defined by the scattering configuration, i.e., $\mathbf{q}=2\mathbf{k}_L-\mathbf{k}_S$, where $\mathbf{k}_L$ and $\mathbf{k}_S$ are the wave vectors of the incident and scattered radiation, respectively. The unit vectors $\hat{\mathbf{e}}_S$ and $\hat{\mathbf{e}}_L$ indicate the electric-field directions chosen by the polarizers and half-wave plates in the path of the laser beam and in front of the entrance slit of the spectrometer. The Fourier transform $\chi^{(2)}(\mathbf{q})$ of the spatially fluctuating second-order susceptibility $\chi^{(2)}(\mathbf{r})$ is given by

$$\chi^{(2)}(\mathbf{q})=\frac{1}{V}\int d\mathbf{r}\,\chi^{(2)}(\mathbf{r})e^{-i\mathbf{q}\mathbf{r}} . \quad (5)$$

Hence the HRL efficiency can be expressed in terms of

$$G_{ijklmn}(\mathbf{q})=\frac{1}{V^2}\int d\mathbf{r}\int d\mathbf{r}'\,\chi^{(2)}_{ijk}(\mathbf{r})\chi^{(2)}_{lmn}(\mathbf{r}')e^{i\mathbf{q}(\mathbf{r}-\mathbf{r}')} , \quad (6)$$

where $\chi^{(2)}$ is assumed to have no imaginary part.

It is straightforward to write down the angular functions describing S_{HRL} as a function of $\hat{\mathbf{e}}_S$ and $\hat{\mathbf{e}}_L$. For the four scattering configurations considered in Fig. 8 we always obtain

$$|\hat{\mathbf{e}}_S\cdot\chi^{(2)}:\hat{\mathbf{e}}_L\hat{\mathbf{e}}_L|^2=C_0+C_2\sin^2\phi+C_4\sin^2\phi\cos^2\phi , \quad (7)$$

where the direction of $\mathbf{e}_L$ is specified by $\phi=\sphericalangle(\mathbf{e}_L,[010])$ and the coefficients C_0, C_2, and C_4 are lengthy combinations of $G_{ijklmn}(\mathbf{q})$.

Since $KTaO_3$ is only an incipient ferroelectric, the region of "critical opalescence" is not reached and the correlation length of the spatial fluctuations of $\chi^{(2)}$ may be always small compared to $1/q$. In the simplest approximation we have

$$G_{ijklmn}(\mathbf{q})\approx G_{ijklmn}(0)=\Gamma_{ijklmn} \quad (8)$$

so that HRL scattering becomes characterized by a sixth-rank tensor satisfying the cubic symmetry.

Expressions for C_0, C_2, and C_4 following from assumption (8) are listed in Table I. The triplets of indices ijk and lmn are contracted according to $1\hat{=}xxx$, $2\hat{=}xyy$, and $3\hat{=}xyz$. Moreover, $\chi^{(2)}_{ijk}(\mathbf{r})$ is regarded to be fully symmetric in its three indices at any point $\mathbf{r}$ (Kleinman's symmetry relations). From Table I and Eq. (7) we expect two easily verifiable properties of the angular functions $I_{\mathrm{HRL}}(\phi)$ describing the variations of the HRL intensity with the laser polarization.

(a) $I_{\mathrm{HRL}}(\phi)$ should be constant for $x(\phi,x)z$ and should be identical for $x(\phi,y)z$ and $x'(\phi,y)z'$, provided $\Gamma_{33}=0$.

(b) The same HRL intensities should be observed for $x(z,y)z$, $x'(z',y)z'$, $x(y,x)z$, and $x'(y,x')z'$ [i.e., $x(\phi,y)z$ and $x'(\phi,y)z'$ at $\phi=90°$, $x(\phi,x)z$ and $x'(\phi,x')z'$ at $\phi=0°$].

We note that similar conditions hold for the HRM intensities of the F_{1u} phonons.[30] While condition (a) is strictly fulfilled, condition (b) has to be slightly modified because the HRM intensities at $x(z,y)z$ and $x'(z',y)z'$ must be twice as strong as the HRM intensities at $x(y,x)z$ and $x'(y,x')z'$.

As illustrated by Fig. 8, conditions (a) and (b) are both satisfied at low temperatures. At higher temperatures, however, condition (b) becomes violated. Thus HRL scattering at low temperatures appears to be independent

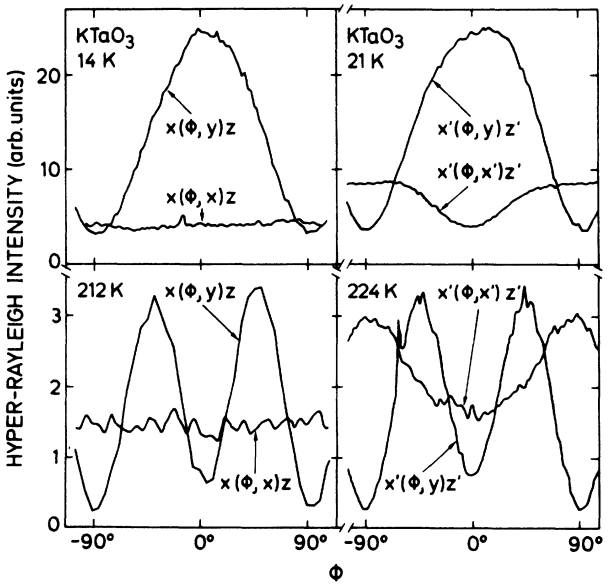

FIG. 8. Variations of hyper-Rayleigh intensity with laser polarization observed for four scattering configurations at the lower and upper end of the temperature range under investigation. The angle ϕ is defined as in Fig. 2. $x'\hat{=}[101]$, $z'\hat{=}[\bar{1}01]$.

TABLE I. Dependence of the hyper-Rayleigh scattering intensity on the polarization of the incident laser radiation denoted by the unit vector $\hat{\mathbf{e}}_L$. We only quote the three coefficients of the angular functions $C_0+C_2\sin^2\phi+C_4\sin^2\phi\cos^2\phi$. For the wave-vector dependent, but temperature-independent scattering (Sec. IV C), the common factor P_{dxx} has been omitted. The cubic axes are denoted by x, y, and z, while x' and z' stand for the [101] and [$\bar{1}$01] directions, respectively.

$\hat{\mathbf{e}}_L$	Scattering configuration	Wave-vector-independent, but temperature-dependent scattering			Wave-vector-dependent, but temperature-independent scattering		
		C_0	C_2	C_4	C_0	C_2	C_4
$(0,\cos\phi,\sin\phi)$	$x(\phi,y)z$	Γ_{11}	$-\Gamma_{11}+\Gamma_{22}$	$-\Gamma_{11}+3\Gamma_{22}+2\Gamma_{12}$	0	0	$2g_{44}^2$
	$x(\phi,x)z$	Γ_{22}	0	$4\Gamma_{33}$	$\frac{1}{2}g_{44}^2$	0	0
$(\sin\phi/\sqrt{2},\cos\phi,-\sin\phi/\sqrt{2})$	$x'(\phi,y)z'$	Γ_{11}	$-\Gamma_{11}+\Gamma_{22}+\Gamma_{33}$	$-\Gamma_{11}+3\Gamma_{22}+2\Gamma_{12}-\Gamma_{33}$	0	0	$2g_{44}^2$
	$x'(\phi,x')z'$	Γ_{22}	$\frac{1}{4}(\Gamma_{11}-3\Gamma_{22}-2\Gamma_{12})$	$\frac{1}{4}(-\Gamma_{11}-9\Gamma_{22}+6\Gamma_{12})$	$\frac{1}{2}g_{44}^2$	$\frac{1}{8}(g_{11}^2-3g_{44}^2-2g_{11}g_{44})$	$\frac{1}{8}(-g_{11}^2-g_{44}^2+6g_{11}g_{44})$

Notation:
$g_{11}=g_{xxxx}, g_{44}=g_{yzyz}, \Gamma_{11}=\Gamma_{xxxxxx}=\Gamma_{11}^{(0)}+P_{xx}g_{11}^2, \Gamma_{22}=\Gamma_{xyxyxy}=\Gamma_2^{(0)}+P_{xx}g_{44}^2, \Gamma_{12}=\Gamma_{xxxyyy}=\Gamma_{12}^{(0)}+P_{xx}g_{11}g_{44}, \Gamma_{33}=\Gamma_{xyzxyz}=\Gamma_{33}^{(0)}$

of $\mathbf{q}$, resulting from scattering centers uncorrelated on the scale of the wavelength of light. At higher temperatures a wave-vector-dependent contribution is superimposed indicating the presence of long-range forces in the form of a macroscopic spatially fluctuating electric field.[36]

B. Low-temperature results

Part of the sixth-rank tensor Γ can be rewritten as a contraction of two fourth-rank tensors if $\chi^{(2)}(\mathbf{r})$ is expanded in terms of the quasistatic polarization $\mathbf{P}(\mathbf{r})$ associated with quasistatic lattice distortions.[7] Defining the polarization-induced contribution to $\chi^{(2)}(\mathbf{r})$ by

$$\Delta_P\chi_{ijk}^{(2)}(\mathbf{r})=\sum_s g_{ijks}P_s(\mathbf{r}) \tag{9}$$

we obtain

$$\Gamma_{ijklmn}=\Gamma_{ijklm}^{(0)}+P_{xx}\sum_s g_{ijks}g_{lmns} \ . \tag{10}$$

Besides charge factors, the fourth-rank tensor g_{ijks} is an appropriate average over HRM tensors. The second-rank tensor $P_{ij}=P_{xx}\delta_{ij}$ is given by

$$P_{ij}=\frac{1}{V^2}\int d\mathbf{r}\int d\mathbf{r}'\,P_i(\mathbf{r})P_j(\mathbf{r}') \ . \tag{11}$$

The tensor $\Gamma^{(0)}$ comprises residuary contributions to Γ, in particular those which might arise from defect cores and cannot be described in terms of variables of the pure crystal.

From the experimental results of Fig. 7 we learn how Γ becomes dominated by the soft mode for $T\to 0$ K. On the one hand, g approaches the soft-mode HRM tensor, i.e.,

$$g_{ijks}\to R_{isjk}\frac{V}{NZ} \ , \tag{12}$$

where N is the number of unit cells within the volume V, Z the transverse effective charge, and $R_{isjk}=\partial\chi_{ijk}^{(2)}/\partial Q_s$ the HRM tensor of the soft mode.[32] On the other hand, we observe

$$P_{xx}\sim\Omega_0^{-4} \ . \tag{13}$$

This power law can readily be explained by the model of randomly distributed microregions of "frozen" soft-mode polarization decaying with increasing distance r from the core according to the well-known Ornstein-Zernike function:

$$g_c(r)=P_0\frac{\xi}{r}e^{-r/r_c} \ . \tag{14}$$

Here, $r_c\sim\Omega_0^{-1}$ is the correlation length of the soft-mode polarization while ξ stands for the radius of the core of the microregion.[8,37] Introducing the average number of microregions per unit volume as concentration c_M, we obtain

$$P_{xx}=\frac{c_M}{V}\left[\int d\mathbf{r}\,g_c(\mathbf{r})\right]^2=\frac{16\pi^2}{V}c_MP_0^2\xi^2r_c^4\sim\Omega_0^{-4} \ . \tag{15}$$

If we want to calculate the HRM intensity of the soft mode in the high-temperature limit, we should write

$$P_{xx}=\frac{P_0}{V}\int d\mathbf{r}\, g_c(\mathbf{r})=\frac{4\pi}{V}P_0^2\xi r_c^2\sim\Omega_0^{-2} \tag{16}$$

because in this case the medium has to be taken as homogeneous and $P_0 g_c(r)$ has to be interpreted as the pair correlation function of the soft-mode polarization. Comparing Eqs. (15) and (16), we clearly recognize the amplification of the HRL intensity by the coherent addition of scattering amplitudes within a microregion.

The order of magnitude of r_c can be estimated from the slope of the soft-mode branch $\Omega(\mathbf{q})$ at the center of the Brillouin zone. As far as $\Omega(\mathbf{q})$ can be approximated by $\Omega^2(\mathbf{q})=\Omega_0^2+D^2q^2$, the correlation length is given by[38]

$$r_c=D/\Omega_0\ . \tag{17}$$

We can deduce this equation within the framework of lattice dynamics, if we assume the Green's function of the phonons to be dominated by the soft-mode contribution and the quasistatic lattice distortions to result from short-range forces localized at a single unit cell. Thus Eq. (17) may certainly be applied to the soft-mode polarization frozen around a symmetry-breaking point defect.

Using the neutron scattering data of Ref. 27, we find r_c to increase from about 5 Å to about 18 Å when the temperature is lowered from 200 to 10 K. These values are in reasonable agreement with the average radius of the microregions determined from the first-order features in the ordinary Raman spectrum.[14] Indeed, first-order Raman and HRL scattering should be explained in terms of the same model because both effects probe the same violations of inversion symmetry.[39] We should admit, however, the limited accuracy of our estimate or r_c due to the anisotropy of the coefficient D. We have taken the value of D for $\mathbf{q}\|[100]$, although D depends on the direction of $\mathbf{q}$, i.e., $D=D(\mathbf{q}/q)$, and an appropriate average has to be inserted into Eq. (17).[14,40] In any case, we have $r_c\ll 1/q$. Continuous-medium models,[8] based on the condition that r_c is large compared to the lattice constant, are not strictly justified although they may be useful approximations for the interpretation of low-temperature data. We further note that for $r_c\approx 18$ Å the microregions can be regarded as isolated only if $(c_M V/N)\ll 3\times 10^{-3}$.

We can obtain additional information about the microregions from the ratio of HRL and HRM intensities. Neglecting $\Gamma_{11}^{(0)}$, we may write for the scattering configuration $x\,(yy)z$

$$\frac{I_{\mathrm{HRL}}}{I_{\mathrm{HRM}}}=\frac{P_{xx}}{\langle P_x^2\rangle}=\left[\frac{c_M V}{N}\right]\frac{\overline{(p_{Mx})^2}}{\langle p_x^2\rangle}\ . \tag{18}$$

In the numerator we average the square of the quasistatic dipole moments $\mathbf{p}_M$ of the microregions, while in the denominator we take the thermal average over the dipole moment $\mathbf{p}$ of the unit cells due to the soft-mode vibration.

At about 10 K we find $I_{\mathrm{HRL}}/I_{\mathrm{HRM}}\approx 1$. By means of Eq. (18) this experimental result can be explained in two entirely different ways.

(i) Using Eq. (14) and expressing $\mathbf{p}_M$ in terms of the dipole moment $\mathbf{p}_0=2\pi\xi^3\mathbf{P}_0$ [integral of $g_c(r)$ over a sphere of radius $\xi\ll r_c$] of the core, we obtain

$$\left[\frac{c_M V}{N}\right]\frac{\overline{(p_{0x})^2}}{\langle p_x^2\rangle}\approx\frac{1}{4}\left[\frac{\xi}{r_c}\right]^4\approx 6\times 10^{-4}\ , \tag{19}$$

where ξ has been identified with the lattice constant. Thus a defect concentration $(c_M V/N)$ of less than 1/1000 and a quasistatic core dipole moment of the order of magnitude of $(\langle p_x^2\rangle)^{1/2}\approx 5\times 10^{-18}$ esu cm are sufficient to account for the observed HRL intensity. In view of the various kinds of defects established in nominally pure samples of $KTaO_3$ (Refs. 41 and 42), a defect model for explaining HRL scattering seems to be rather suitable.

(ii) Following Ref. 13, we may imagine spontaneously formed symmetry-breaking microregions independent of any defect. Then it is natural to assume $1/c_M\rightarrow v_c=(4\pi/3)r_c^3$ for $T\rightarrow 0$ K and to introduce the average dipole moment of a unit cell within a microregion by $\overline{p_x}=[(p_{Mx})^2]^{1/2}/[(N/V)/v_c]$. We obtain

$$\overline{p_x}\rightarrow\left[\frac{c_M V}{N}\right]^{1/2}(\langle p_x^2\rangle)^{1/2}\approx 5\times 10^{-2}(\langle p_x^2\rangle)^{1/2}\ . \tag{20}$$

The off-center displacement corresponding to $\overline{p_x}$ turns out to have the same order of magnitude as that derived in Ref. 13 ($\delta=0.04$ Å), so that our experimental results can also be interpreted in terms of a glass-type behavior, randomly oriented microregions of radius r_c filling the whole crystal volume for $T\rightarrow 0$ K.

The possibility of explaining our data by different models clearly demonstrates that HRL scattering at low temperatures only proves the existence of quasistatic soft-mode-type lattice distortions, but tells almost nothing about their origin, their core, or the preferential directions of their polarization.

C. High-temperature results

In the preceding section we neglected the macroscopic electric field associated with any quasistatic polarization. Instead of Eq. (14), we should have written[8,43]

$$\mathbf{P}(\mathbf{r})=\mathbf{P}_0\frac{\xi}{r}e^{-r/r_c}+r_c^2\xi(\mathbf{P}_0\cdot\nabla)\nabla\left[\frac{1-e^{r/r_c}}{r}\right] \tag{21}$$

for describing the decrease of the frozen soft-mode polarization with increasing distance from the core of the microregion. The lattice-dynamics analogue to Eq. (21) can be derived under the same assumptions [short-range forces restricted to a single unit cell, dominance of the soft-mode contributions to the Green's function, $\Omega^2(\mathbf{q})=\Omega_0^2+D^2q^2$] as Eqs. (14) and (17), provided that the TO-LO splitting is properly taken into account and soft-mode contributions to the Green's function are excluded for phonon eigenvectors parallel to $\mathbf{q}$. Since the Fourier transform of the additional second term in Eq. (21) depends on the direction of $\mathbf{q}$, even for $\mathbf{q}\rightarrow\mathbf{0}$, a wave-vector-dependent HRL scattering is predicted which should vary with temperature as r_c^4. Such a scattering, however, is not observed, so that we must as-

sume the feedback on the quasistatic lattice distortions via their own macroscopic electric field to be wiped out either by superposition of the random electric fields of the neighboring microregions or by interference with the anisotropy of D in $\mathbf{q}$ space.

Besides short-range forces, defects exert long-range forces on the host lattice due to the electric field of their charge distributions, especially their dipole moments. Assuming the latter to be rigid and taking into account the equations of electrostatics, we may express the Fourier transform of the resulting macroscopic field by[36]

$$\mathbf{E}(\mathbf{q})=-\frac{4\pi}{\epsilon_s q^2}[\mathbf{P}_d(\mathbf{q})\cdot\mathbf{q}]\mathbf{q} \ . \tag{22}$$

Here, ϵ_s is the static dielectric constant and $\mathbf{P}_d$ the defect polarization, i.e., the sum of the rigid dipole moments of the defects per unit volume. Note that $\mathbf{P}_d$ has to be distinguished from $\mathbf{P}_0$ characterizing the soft-mode polarization of the core of a microregion or, to state it more precisely, the coupling between the core and the quasistatic soft-mode polarization of the surrounding host lattice.

We expect $\mathbf{E}(\mathbf{q})$ to give rise to electric-field-induced SHG (ESHG). While in common ESHG experiments the voltage across the crystal is kept constant and the intensity varies with $\epsilon_s^2\sim\Omega_0^{-4}$, the present situation corresponds to an ESHG experiment where the charges on the plates of the capacitor filled with the crystal are fixed and the temperature dependence of ESHG is suppressed by the screening factor $1/\epsilon_s$. Indeed, the electro-optic contribution to $G_{ijklmn}(\mathbf{q})$ due to $\mathbf{E}(\mathbf{q})$ may be written as

$$\Delta_{\rm eo}G_{ijklmn}(\mathbf{q})=\left[\frac{\epsilon_s-1}{\epsilon_s}\right]^2 P_{dxx}\sum_{s,s'}g_{ijks}g_{lmns'}\frac{q_s q_{s'}}{q^2} \ , \tag{23}$$

where P_{dxx} is defined in the same way as P_{xx}.

The expressions for C_0, C_2, and C_4 following from Eq. (23) are listed in Table I. Although the agreement is still far from perfect, the high-temperature results of Fig. 8 seem to approach these predictions. Especially, we notice the dominance of the C_4 term in the scattering configurations $x(\phi,y)z$ and $x'(\phi,y)z'$. In an improved analysis we have to take into account the superposition and interference of the two HRL scattering mechanisms specified by Eqs. (10) and (22).

V. CONCLUSIONS

We have singled out two contributions to HRL scattering from the bulk of nominally pure $KTaO_3$.

(a) There is a wave-vector-independent, but strongly temperature-dependent contribution which arises from microregions of quasistatic soft-mode polarization expanding with decreasing temperature proportionally to the inverse of the soft-mode frequency.

(b) There is a wave-vector-dependent, but temperature-independent contribution resulting from the macroscopic electric field associated with the dipole moments of defects.

Further clarification requires at least two natural extensions of our work.

(i) HRL scattering should be studied from samples containing defined defects of controlled concentration.

(ii) Since elaborate shell models of $KTaO_3$ are available,[44] it should be possible to describe the quasistatic distortions probed by HRL scattering in terms of concrete models of lattice dynamics or statics.

Attempts in these directions are in progress.

ACKNOWLEDGMENTS

The author wishes to thank M. Cardona, D. Rytz, and K. Syassen for a critical reading of the manuscript, and H. Hirt, M. Siemers, and P. Wurster for technical help. He is particularly indebted to D. Rytz (Hughes Research Laboratories, Malibu, California) and H. Uwe (Institute of Applied Physics, University of Tsukuba, Japan) for providing samples of $KTaO_3$. The support of the Deutsche Forschungsgemeinschaft (Bonn, Germany) is gratefully acknowledged.

[1]M. J. French, in *Chemical Applications of Nonlinear Raman Spectroscopy*, edited by A. B. Harvey (Academic, New York, 1981), p. 239.

[2]H. Vogt, in *Light Scattering in Solids II*, Vol. 50 of *Topics in Applied Physics*, edited by M. Cardona and G. Güntherodt (Springer, Berlin, 1982), p. 207.

[3]V. N. Denisov, B. N. Mavrin, and V. B. Podobedov, Phys. Rep. **151**, 1 (1987).

[4]K. Inoue, Ferroelectrics **52**, 253 (1983); Jpn. J. Appl. Phys. **24**, Suppl. 24-2, 107 (1985).

[5]H. Vogt and H. Uwe, Phys. Rev. B **29**, 1030 (1984).

[6]H. Vogt, M. D. Fontana, G. E. Kugel, and P. Günter, Phys. Rev. B **34**, 410 (1986).

[7]A. P. Levanyuk, A. I. Morozov, and A. S. Sigov, Fiz. Tverd. Tela (Leningrad) **28**, 436 (1986) [Sov. Phys.—Solid State **28**, 242 (1986)].

[8]A. P. Levanyuk, V. V. Osipov, A. S. Sigov, and A. A. Sobyanin, Zh. Eksp. Teor. Fiz. **76**, 345 (1975) [Sov. Phys.—JETP **49**, 176 (1979)].

[9]N. I. Lebedev, A. P. Levanyuk, A. I. Morozov, and A. S. Sigov, Fiz. Tverd Tela (Leningrad) **25**, 2979 (1983) [Sov. Phys.—Solid State **25**, 1719 (1983)].

[10]A. I. Isaverdiev, A. P. Levanyuk, A. I. Morozov, and A. S. Sigov, Fiz. Tverd Tela (Leningrad) **30**, 2104 (1988) [Sov. Phys.—Solid State **30**, 1213 (1988)].

[11]J. P. Sokoloff, L. L. Chase, and D. Rytz, Phys. Rev. B **38**, 597 (1988).

[12]M. Maglione, S. Rod, and U. T. Höchli, Europhys. Lett. **4**, 631 (1987).

[13]S. Rod, F. Borsa, and J. J. van der Klink, Phys. Rev. B **38**, 2267 (1988).

[14]H. Uwe, K. B. Lyons, H. L. Carter, and P. A. Fleury, Phys. Rev. B **33**, 6436 (1986).

[15]B. I. Halperin and C. M. Varma, Phys. Rev. B **14**, 4030 (1976).

[16]P. S. Pershan, Phys. Rev. **130**, 919 (1963).

[17]V. N. Denisov, B. N. Marvin, V. B. Podobedov, Kh. E. Sterin, and B. G. Varshal, Opt. Spektrosk. **49**, 406 (1980) [Opt. Spectrosc. (USSR) **49**, 221 (1981)].

[18]H. Vogt and G. Neumann, Phys. Status Solidi B **86**, 615 (1978).
[19]S. Shin, A. Ishida, T. Yamakami, T. Fujimura, and M. Ishigame, Phys. Rev. B **35**, 4455 (1987).
[20]S. Shin, M. Ishigame, K. Deguchi, and E. Nakamura, Solid State Commun. **65**, 749 (1988).
[21]H. Vogt and H. Presting, Phys. Rev. B **31**, 6731 (1985).
[22]S. Shin and M. Ishigame, Phys. Rev. B **34**, 8875 (1986).
[23]Y. Morioka, M. Wada, and A. Sawada, J. Phys. Soc. Jpn. **57**, 3198 (1988).
[24]K. Inoue, A. Hasagawa, K. Watanabe, H. Yamagushi, H. Uwe, and T. Sakudo, Phys. Rev. B **38**, 6352 (1988).
[25]M. J. French, R. J. B. Hall, D. A. Long, and F. M. F. Al-Rubaiey, J. Raman Spectrosc. **16**, 398 (1985).
[26]H. H. Barrett, Phys. Rev. **178**, 743 (1969).
[27]J. D. Axe, J. Harada, and G. Shirane, Phys. Rev. B **1**, 1227 (1970).
[28]I. M. Buzin, I. V. Ivanov, and V. A. Chistyaev, Fiz. Tverd. Tela (Leningrad) **22**, 2848 (1980) [Sov. Phys.—Solid State **22**, 1662 (1980)].
[29]Samples have been provided by H. Uwe, Institute of Applied Physics, University of Tsukuba, Japan, and D. Rytz, Hughes Research Laboratories, Malibu, California 90265.
[30]H. Vogt, Phys. Rev. B **38**, 5699 (1988).
[31]W. Kleemann and F. J. Schäfer, Jpn. J. Appl. Phys. **24**, Suppl. 24-2, 260 (1985).
[32]H. Vogt, Phys. Rev. B **36**, 5001 (1987).
[33]H. Vogt, J. A. Sanjurjo, and G. Rossbroich, Phys. Rev. B **26**, 5904 (1982).
[34]H. Vogt and G. Neumann, Phys. Status Solidi B **92**, 57 (1979).
[35]Y. Fujii and T. Sakudo, Phys. Rev. B **13**, 1161 (1976).
[36]V. L. Ginzburg, A. P. Levanyuk, and A. A. Sobyanin, Phys. Rep. **57**, 151 (1980).
[37]R. Blinc and B. Žekš, *Soft Modes in Ferroelectrics and Antiferroelectrics* (North-Holland, Amsterdam, 1974), p. 34.
[38]R. J. Elliott, in *Structural Phase Transitions and Soft Modes*, edited by E. J. Samuelsen, E. Andersen, and J. Feder (Universitetsforlaget, Oslo, 1971), p. 235.
[39]H. Uwe, Jpn. J. Appl. Phys. **24**, Suppl. 24-2, 513 (1985).
[40]R. Comès and G. Shirane, Phys. Rev. B **5**, 1886 (1972).
[41]D. Houde and S. Jandl, Solid State Commun. **60**, 45 (1986).
[42]P. Grenier, G. Bernier, S. Jandl, B. Salce, and L. A. Boatner, J. Phys. Condens. Matter **1**, 2515 (1989).
[43]A. P. Levanyuk, V. V. Osipov, and A. S. Sigov, Ferroelectrics **18**, 147 (1978).
[44]C. H. Perry, R. Currat, H. Buhay, R. M. Migoni, W. G. Stirling, and J. D. Axe, Phys. Rev. B **39**, 8666 (1989).